State Selective Dynamics of TiO_2 Charge Carrier Trapping and Recombination

Yu Zhang, [†,‡,§] *Daniel T. Payne,* [†,‡] *Chi L. Pang,* [†,‡] *Cephise Cacho,* [§] *Richard T. Chapman,* [§] *Emma Springate,* [§] *Helen H. Fielding,* [†] *and Geoff Thornton* [†,‡,*]

[†]Department of Chemistry, 20 Gordon Street, University College London, London WC1H 0AJ, UK

[‡]London Centre for Nanotechnology, 17-19 Gordon Street, University College London, London WC1H 0AH, UK

[§]Central Laser Facility, STFC Rutherford Appleton Laboratory, Didcot OX11 0QX, UK

*E-mail: g.thornton@ucl.ac.uk.

Abstract:

Time-resolved pump-probe photoemission spectroscopy has been used to study the dynamics of charge carrier recombination and trapping on hydroxylated rutile TiO_2(110). Two types of pump excitation were employed, one in the infrared (0.95 eV) and the other in the UV (3.5 eV) region. With IR excitation, electrons associated with defects are excited into the bottom of the conduction band from the polaronic states within the band gap, which are retrapped within 45±10 fs. Under UV excitation, the electrons in these band gap state (BGS) and valence band electrons are excited into the conduction band. In addition to the fast polaron trapping observed with IR excitation, we also observe a long lifetime (about 1 ps) component to both the depletion of hot electrons at the bottom of the conduction band and the refilling of the BGS. This points to a BGS mediated recombination process with a ps lifetime.

Table of Contents image:

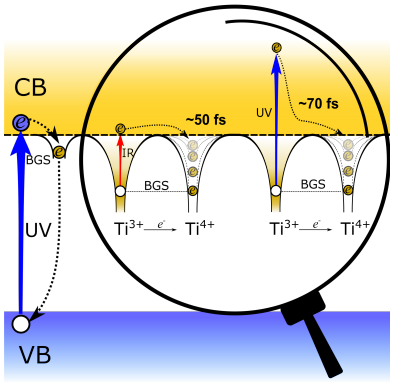

The recombination pathways of charge carriers are of paramount importance in photocatalysis because they determine the lifetime of chemically active sites, and hence the catalytic efficiency. These pathways are not known in detail even for a prototypical material such as TiO_2, in part because of challenges associated with the presence of polaronic trapping centres[1–8]. The relationship between the associated trapping processes and the charge carrier recombination dynamics is important in a number of applications of TiO_2 in addition to photocataysis, such as its use as an electron collector in perovskite solar cells[9].

The study of the recombination dynamics in TiO_2 has so far relied on techniques such as photoluminesence and transient absorption spectroscopy (TAS) [10,11]. Both techniques have provided valuable results down to the fs regime, with TAS allowing the dynamics of electrons and holes to be examined independently. However, neither method can monitor the recombination in a state selective manner, which is achieved in this work through the use of time-resolved femtosecond pump-probe photoemission spectroscopy.

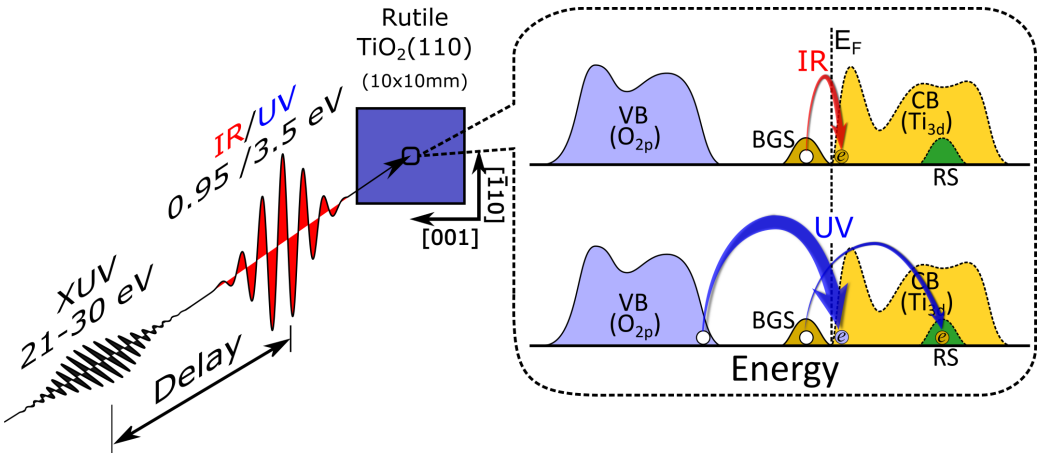

Figure. 1 Scattering geometry of the pump probe experiments, with light incident at 45˚ to the surface normal in the [001] azimuth. The pump electric field of the incident light is parallel to the [$\bar{1}$10] azimuth. The dashed box shows the excitation routes for IR and UV pumped experiments. IR can excite electrons from the band gap states (BGS) to the bottom of the conduction band (CB), while UV can

excite electrons both from the BGS to a resonance state (RS) in the conduction band (small arrow) and from the valence band (VB) to the conduction band (large arrow).

A schematic diagram of the valence band and conduction band density of states of hydroxylated rutile TiO_2 is shown in Figure 1[12]. The accepted picture of TiO_2 photocatalysis involves photoexcitation of electrons across the 3 eV band gap[13]. More recently, a second photoabsorption channel with a threshold at about 3 eV has been identified, although it is not yet clear what, if any, role it plays in photocatalysis[14–16]. This channel involves excitation from the polaronic Ti 3d BGS, which have an apparent binding energy of 0.8 eV, into a resonance in the conduction band that lies 3.5 eV above. In this study we investigate the recombination of charge carriers and electron trapping associated with the valence and conduction bands as well as the BGS. The results point to the importance of the BGS in both fast and slow decay of hot charge carriers. BGS not only absorb photons and form transient excited states, but also trap band electrons and holes to accelerate recombination.

The excitation processes are shown schematically in Figure 1. In the IR-pumped experiment, a photon energy of 0.95 eV is chosen to be close to the resonance energy, 0.8 eV, found in previous IR absorption experiments[2,17]. This energy allows BGS electrons to be excited to the bottom of the conduction band, after which they become retrapped in the polaronic BGS. The delayed probe pulse then monitors the change of the BGS and the bottom of the conduction band by photoemission in order to measure the dynamics of the retrapping process. In the second experimental scheme, a photon energy of 3.5 eV is employed as the pump. From previous band gap measurements and calculations[18,19], this energy is well above the band gap of about 3 eV, and known to match a band gap absorption in rutile TiO_2. As noted above, this energy is also associated with the excitation from the BGS to a resonance state within the conduction band[14–16], which has been interpreted differently as hydroxyl induced states[16] or

higher Ti 3d states[14,15]. A comparison between the dynamics induced by IR and UV pulses allows us to separate the dynamics of polarons from that of band electrons and holes. (See Supporting information S1 for experimental details.)

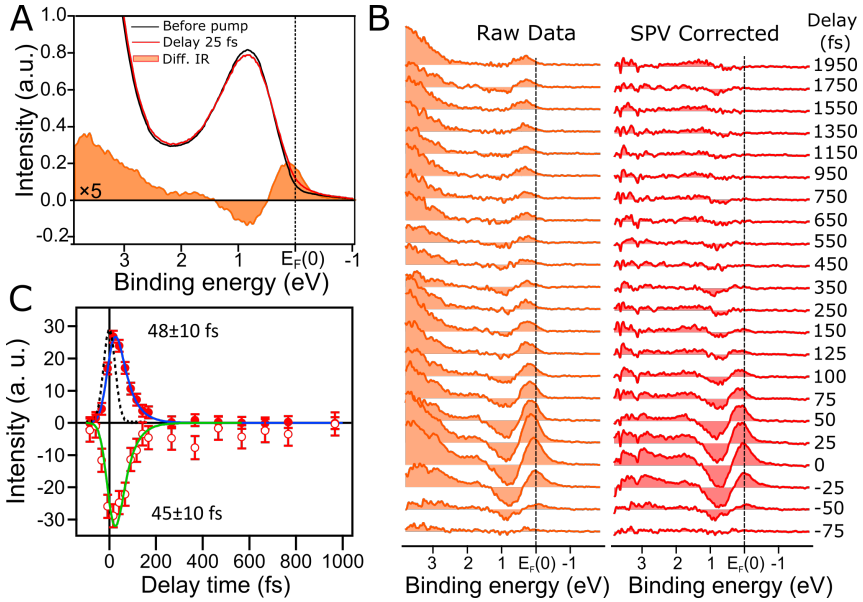

Figure 2. A Photoemission spectra (hν = 20.9 eV) before the IR pump pulse (black) and at a delay time of 25 fs (red). The difference between the two spectra is shown as the filled spectrum. **B** The difference spectra measured at different delay times. Left panel shows the raw data. The difference spectra after the correction for the surface photovoltage (SPV) effect (shifting the delayed spectra by about 10 meV) are shown on the right. **C** The evolution of hot electrons (filled circles) at E_F and recovery of the BGS peak (open circles) as a function of delay time. The intensities are obtained from the difference within an energy window of 0.3 eV centred at 0 eV binding energy (hot electrons around E_F) and 0.9 eV (band gap state) binding energy, respectively. A single exponential decay function convolved with the cross correlation function (black dashed curve) is employed to fit the data.

Figure 2A shows the photoemission spectra of the top of the valence band, the BGS and the bottom of the conduction band in IR-pumped experiments. The black and red curves are the spectra measured before the arrival of pump pulses (referred to as a steady state spectrum) and at a delay time of 25 fs, respectively. The peak at about 0.8 eV binding energy is from the

BGS. The upper edge of the valence band is seen at binding energies above 3 eV. In the time-delayed spectrum (red), the introduction of the IR pump laser causes a significant decrease of the BGS peak intensity and an increase in intensity around E_F. These changes can be clearly seen in the corresponding difference spectrum in the same graph. A depletion of the BGS is indicated by the negative peak at 0.8 eV, and population of hot electrons gives rise to a positive peak at around E_F. It should be noted that the excited hot electrons should in principle lie above E_F. However, due to the instrumental broadening their distribution appears to be centered at E_F. For binding energies larger than 2 eV, there is an unexpectedly large positive increase in the difference spectrum. This is mainly attributed to a shift of the valence band caused by the relaxation of surface band bending, a phenomenon known as the surface photovoltage (SPV) effect[20]. It is commonly observed for semiconductor surfaces in pump-probe measurements and has also been observed on TiO_2[21]. In this case the (red) spectrum shifts to a slightly higher energy, giving rise to a significant positive contribution in the difference spectrum where the valence band rises. To compensate for the SPV effect we shift all the IR pumped spectra to lower binding energy. The magnitude of the shift, typically about 10 meV, is determined from the SPV shift measured at around 3 eV binding energy (Supporting information S2).

Figure 2B shows the difference spectra calculated from the raw data (left) and SPV compensated data (right) for different delay times of IR pump pulses. Compensating for SPV has the effect of removing the positive excursions below 3 eV for all delay times. It also removes small positive excursions around E_F for delay times longer than 250 fs. The SPV compensation allows us to resolve the trapping dynamics with high accuracy. It also reveals a time dependence of the intensity between 1 and 3 eV binding energy around zero time delay, which is attributed to a change of secondary electron background arising from the elevated electron temperature. (Supporting information S3).

The dynamics of BGS depletion and hot electron population around E_F is plotted in Figure 2C. An exponential decay function convolved with a Gaussian was applied to fit the data. The Gaussian represents the cross correlation of the IR and XUV pulses, which was obtained from a laser-assisted photoelectric effect measurement[22]. The recovery of the depleted BGS gives an exponential time constant of 45±10 fs. The error arises mainly from the uncertainty in the value of time zero. Hot electron decay has a very similar lifetime of 48±10 fs, as expected on the basis of the trapping model shown in Figure 1 C.

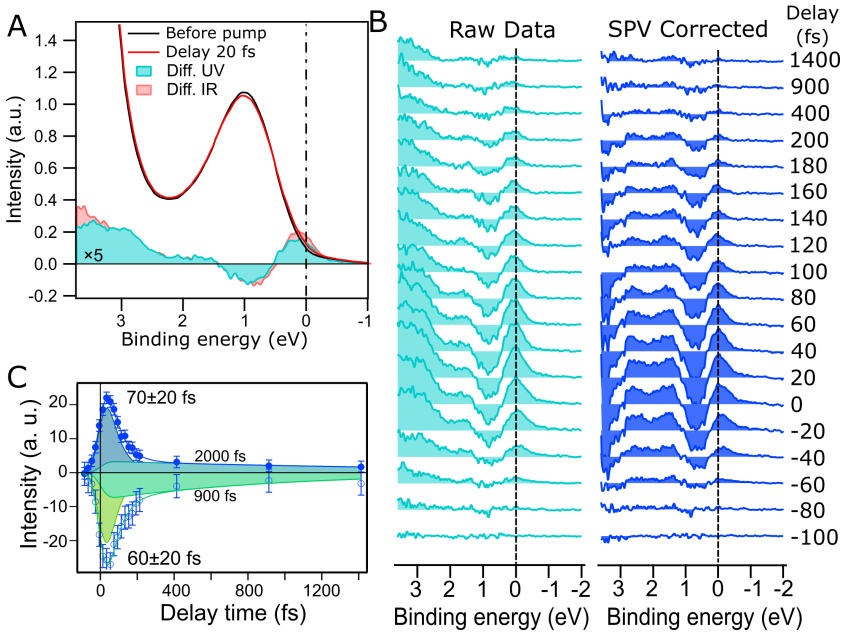

Figure 3. A Photoemission spectra (hν = 30.4 eV) before the UV pump pulse (black) and at a delay time of 20 fs (red). The difference between the two spectra is shown as the filled spectrum. As a comparison, the difference from the IR pumped experiments (delay time 25 fs) is also shown. **B** The difference spectra measured at different delay times. Left panel shows the raw data. The difference spectra after the correction for the SPV effect (shifting the delayed spectra by about 10 meV) are shown on the right. **C** The evolution of hot electrons at E_F and recovery of the BGS peak as a function of delay time. The intensities are obtained from the difference spectra within an energy window of 0.3 eV

centred at 0.9 eV binding energy (open circles) and 0 eV (filled circles) binding energy, respectively. Two exponential decay functions convolved with the cross correlation function are used to fit the data.

In the UV pumped measurements, an increase of hot electrons around E_F and a decrease of electrons at the top of the valence band are expected in the difference spectra. A depletion of BGS is also expected, being associated with the excitation of electrons to an energy of about 2.7 eV above E_F in the conduction band. These electrons are expected to quickly decay back to the bottom of the conduction band (<15 fs) [23,24], joining those excited from the valence band. The population of hot electrons higher in the conduction band is found to be extremely low even at the 0 fs delay time (Supporting information S4). Hence, the spectra in Figure 3 are terminated at about 2 eV above E_F.

In Figure 3A, the increase of hot electrons around E_F can be unambiguously identified, but the depletion at the valence band edge is complicated by the SPV effect. Difference spectra from both IR- and UV-pumped measurements are shown for a 20 fs delay time in Figure 3A. At binding energies greater than 3 eV the positive peak in the IR spectrum will be due solely to the SPV effect. This contrasts with the UV spectrum, where there is a clear depletion at 3.5 eV binding energy. The difference spectra obtained by shifting the delayed spectra to correct for the SPV effect are shown in Figure 3B. This correction makes the assumption that the difference spectra at binding energies less than 3 eV is dominated by the SPV effect (Supporting information S2). Quantitative analysis of the depletion at the valence band edge is not feasible because of uncertainty in the SPV compensation. Nevertheless, it is clear that there is a reduction at 3 eV binding energy consistent with our expectations.

Further analysis of the time dependence of the UV-pumped spectra (Figure 3C) shows that the decay of hot electrons around E_F and the recovery of the BGS behave in a similar manner as in the IR pumped spectra. However, in contrast to the IR-pumped data, both also contain a long decay component. In fitting the recovery of the BGS to two exponential decay components, one has a lifetime of 60±20 fs while the other is of the order of ps. The corresponding values for the hot electron decay are 70±20 fs and 2±2 ps. The large error bars on the fast components include the estimation of time zero, which for the UV pumped data is obtained from the correlation spectrum of the hot electrons at 1 eV above the E_F[14,24,25]. The fitting results of the long decay component have large uncertainties due to the correction of the SPV effect. However, the ps lifetime obtained from the recovery of BGS is little influenced by an SPV effect as the dynamics are calculated around the BGS peak position where the derivative is zero.

The polaron trapping time of conduction band electrons has been estimated from the period of the longitudinal optical (LO) phonon mode[26] that interacts significantly with electron transport. In rutile TiO_2, the energy of this mode is 96 meV[26,27], corresponding to a period of 43 fs. This agrees well with the trapping time observed in our IR-pumped measurements. We can also correlate our results with measurements of anatase TiO_2, where the LO phonon energy of 100 meV is close to that in rutile[28]. For anatase, it is known from resonant inelastic X-ray spectroscopy that the electron polarons are associated with LO phonons. A similar trapping time of electrons in anatase TiO_2 is therefore expected, with a 50 fs lifetime being observed in IR TAS measurements of dye-sensitised TiO_2 thin films[29]. A comparison with the results presented here suggests that this arises from polaron trapping.

We now turn to the depletion and recovery of the BGS peak in the UV-pumped experiments. The fast component of the BGS recovery (60±20 fs) is close to that observed in the IR-pumped experiment (45±10 fs), suggesting that they arise from a similar trapping process. The slightly longer recovery time of about 20 fs in the UV-pumped experiment may be attributed to the additional decay of hot electrons from a higher energy, about 2.7 eV above the E_F, to the bottom of conduction band. Theoretical calculations have investigated this relaxation process in terms of both electron-phonon [24] and electron-electron scattering[30]. The results indicate that the excess energy of hot electrons dissipates into phonons and electron-hole excitations near the Fermi level in a few tens of fs. Since these electrons are originally from localised BGS, they have a high possibility of being retrapped into polaronic states in an additional 45±10 fs.

There are two potential contributions to the long component of the BGS recovery. One is due to the recombination of BGS electrons with valence band holes. This is thought to give rise to photoluminescence with a ns lifetime at about 2.2 eV, significantly smaller than the band gap of 3 eV[11]. The second contribution, which will also affect the decay of hot electrons, arises from the lifetime of band electrons at the bottom of the conduction band being extended by up to a picosecond because of the reduced scattering probability of phonons[24].

The population of hot electrons around E_F is of a similar magnitude to the decrease of BGS intensity at all delay times after UV excitation (Figure 3 B,C). At first sight this is surprising since a dominance of hot electrons created by band-gap-excitation might be expected. There are two likely factors contributing to this apparent anomaly. Firstly, the resonance nature of the BGS to conduction band excitation. Secondly, for 3.5 eV excitation the valence band density of states accessed is not significantly higher than the BGS. This is evidenced by the spectral intensity in Figure 3A, coupled with knowledge that the

photoionisation cross sections of O 2p and Ti 3d are comparable at a photon energy of about 30 eV[31].

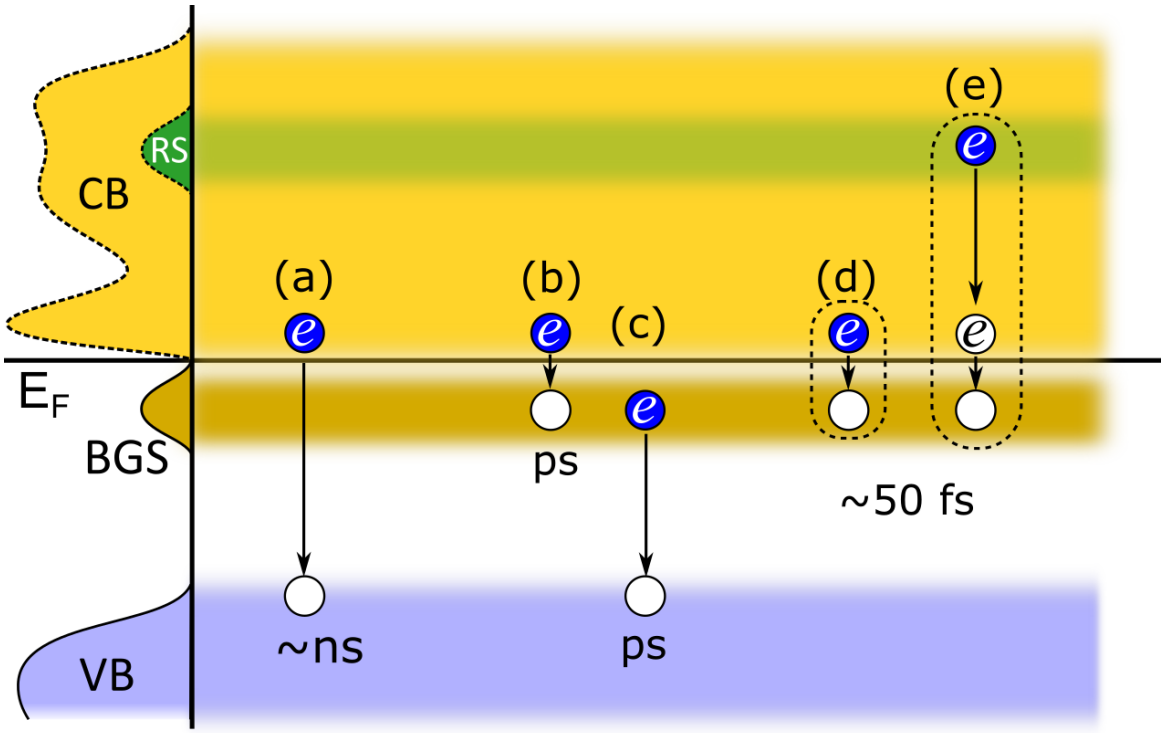

Figure 4. Recombination processes on TiO_2 in order of increasing recombination rate: (a) Direct recombination of band electrons and holes created by band gap excitation; (b) trapping of band electrons created by band gap excitation as polarons; (c) recombination of BGS electrons with valence band holes created by band gap excitation; (d) localised electrons excited from the BGS are retrapped as polarons; (e) similar to (d) but the electrons are first excited from the BGS to the resonance state (RS) in the conduction band, then decay rapidly to lower energies and are finally trapped as polarons. The approximate lifetimes are indicated. The dashed boxes indicate the localised nature of the transitions.

The charge trapping and recombination processes in TiO_2 are summarised graphically in Figure 4. The slowest process is expected to arise from direct recombination of band electrons and holes. There are photoconductivity measurements of TiO_2 that present indirect evidence of conduction band electron recombination with valence band holes, with a recombination lifetime ranging from picoseconds to ns regime[32,33]. A ns lifetime is outside of the temporal range that our experiment can access. It has been also argued that defects can trap and

annihilate carriers in the conduction and valence bands on the ps timescale[10]. Recent calculations also suggest that excess electrons in polaronic states can greatly accelerate the recombination of the electron hole pairs from ns down to a few ps[34]. Related processes in our work are shown schematically in the middle of Figure 4 in b and c. Process c causes the depletion of BGS, while process b refills them. On the basis of the Shockley-Read-Hall model, the involvement of holes will dominate the recombination processes in an n-type semiconductor since they are the minority carrier[35]. Therefore, processes b and c are correlated but the rate of the BGS refilling will be determined by the rate of BGS electron recombination with valence band holes[35]. These two processes have been directly identified here from the long time component of the dynamics of the hot electrons and BGS, as demonstrated in Figure 3B for UV pumped experiments. The fastest dynamics are associated with trapping of excited electrons in the polaronic BGS. A short lifetime for the two processes involved, represented by d and e in Figure 4, presumably arises from the localised nature of the trapping events.

In summary, we have distinguished the recombination processes on the surface of h-TiO_2(110) by measuring the dynamics of relevant states. This was made possible through the use of time resolved IR/UV-pump XUV-probe spectroscopy to measure the state-resolved dynamics. The most rapid electron dynamics are associated with re-trapping of hot electrons created by excitation of polaronic band gap electrons, which is consistent with strong electron-phonon and electron-electron scattering[24]. This makes TiO_2 an excellent material for collecting electrons in dye sensitized and organic perovskite solar cells since the injected electrons are rapidly deexcited to the bottom of the conduction where they will be trapped as mobile polarons by Ti atoms in the bulk. On the other hand, electron trapping into polaronic BGS accelerates the recombination of band electrons and holes created by UV irradiation. Our studies highlight the importance of band gap states in the photo-catalysis and photo-chemistry of TiO_2.

Acknowledgements

This work was supported by the European Research Council Advanced Grant ENERGYSURF (GT), EPSRC (UK) (EP/D068673/1), EU COST Action CM1104, and the Royal Society (UK) through a Wolfson Research Merit Award to GT.

Supporting Information paragraph

Experimental setup and sample preparation; correction of the surface photovoltage effect; the secondary electron emission background; dynamics of hot electrons in higher conduction band. This material is available free of charge via the Internet at http://pubs.acs.org.

References

(1) Austin, I. G.; Mott, N. F. Polarons in Crystalline and Non-Crystalline Materials. *Adv. Phys.* **1969**, *18* (71), 41–102.

(2) Bogomolov, V. N.; Firsov, Y. A.; Kudinov, E. K.; Mirlin, D. N. On the Experimental Observation of Small Polarons in Rutile (TiO_2). *Phys. Stat. Sol.* **1969**, *35* (2), 555–558.

(3) Hendry, E.; Wang, F.; Shan, J.; Heinz, T. F.; Bonn, M. Electron Transport in TiO_2 Probed by THz Time-Domain Spectroscopy. *Phys. Rev. B* **2004**, *69* (8), 081101.

(4) Deskins, N. A.; Dupuis, M. Electron Transport via Polaron Hopping in Bulk TiO_2: A Density Functional Theory Characterization. *Phys. Rev. B* **2007**, *75*, 195212.

(5) Mattioli, G.; Alippi, P.; Filippone, F.; Caminiti, R.; Amore Bonapasta, A. Deep versus Shallow Behavior of Intrinsic Defects in Rutile and Anatase TiO_2 Polymorphs. *J. Phys. Chem. C* **2010**, *114* (49), 21694–21704.

(6) Janotti, A.; Franchini, C.; Varley, J. B.; Kresse, G.; Van de Walle, C. G. Dual Behavior

of Excess Electrons in Rutile TiO_2. *Phys. Status Solidi RRL* **2013**, *7* (3), 199–203.

(7) Deák, P.; Aradi, B.; Frauenheim, T. Polaronic Effects in TiO_2 Calculated by the HSE06 Hybrid Functional: Dopant Passivation by Carrier Self-Trapping. *Phys. Rev. B* **2011**, *83*, 155207.

(8) Yim, C. M.; Chen, J.; Zhang, Y.; Shaw, B.-J.; Pang, C. L.; Grinter, D. C.; Bluhm, H.; Salmeron, M.; Muryn, C. A.; Michaelides, A.; et al. Visualization of Water-Induced Surface Segregation of Polarons on Rutile TiO_2 (110). *J. Phys. Chem. Lett.* **2018**, *9* (17), 4865–4871.

(9) Bi, D.; Tress, W.; Dar, M. I.; Gao, P.; Luo, J.; Renevier, C.; Schenk, K.; Abate, A.; Giordano, F.; Correa Baena, J.-P.; et al. Efficient Luminescent Solar Cells Based on Tailored Mixed-Cation Perovskites. *Sci. Adv.* **2016**, *2* (1), 1501170.

(10) Sachs, M.; Pastor, E.; Kafizas, A.; Durrant, J. R. Evaluation of Surface State Mediated Charge Recombination in Anatase and Rutile TiO2. *J. Phys. Chem. Lett.* **2016**, *7*, 3742–3746.

(11) Yamada, Y.; Kanemitsu, Y. Blue Photoluminescence of Highly Photoexcited Rutile TiO_2: Nearly Degenerate Conduction-Band Effects. *Phys. Rev. B* **2010**, *82*, 113103.

(12) Tezuka, Y.; Shin, S.; Agui, A.; Fujisawa, M.; Ishii, T. Resonant Soft X-Ray Emission Study of Rutile (TiO_2). *J. Phys. Soc. Jpn.* **1996**, 65, 312–317.

(13) Fujishima, A.; Zhang, X.; Tryk, D. A. TiO_2 Photocatalysis and Related Surface Phenomena. *Surf. Sci. Rep.* **2008**, *63* (12), 515–582.

(14) Argondizzo, A.; Cui, X.; Wang, C.; Sun, H.; Shang, H.; Zhao, J.; Petek, H. Ultrafast Multiphoton Pump-Probe Photoemission Excitation Pathways in Rutile TiO_2(110). *Phys. Rev. B* **2015**, *91* (15), 155429.

(15) Wang, Z.; Wen, B.; Hao, Q.; Liu, L.-M.; Zhou, C.; Mao, X.; Lang, X.; Yin, W.-J.; Dai, D.; Selloni, A.; et al. Localized Excitation of Ti^{3+} Ions in the Photoabsorption and

Photocatalytic Activity of Reduced Rutile TiO_2. *J. Am. Chem. Soc.* **2015**, *137* (28), 9146–9152.

(16) Zhang, Y.; Payne, D. T.; Pang, C. L.; Fielding, H. H.; Thornton, G. Non-Band-Gap Photoexcitation of Hydroxylated TiO_2. *J. Phys. Chem. Lett.* **2015**, *6* (13), 3391–3395.

(17) Khomenko, V. M.; Langer, K.; Rager, H.; Fett, A. Electronic Absorption by Ti^{3+} Ions and Electron Delocalization in Synthetic Blue Rutile. *Phys. Chem. Miner.* **1998**, *25* (5), 338–346.

(18) Vos, K. Reflectance and Electroreflectance of TiO_2, Single Crystals II: Assignment to Electronic Energy Levels. *J. Phys. C Solid State Phys.* **1977**, *10*, 3917.

(19) Chiodo, L.; García-Lastra, J. M.; Iacomino, A.; Ossicini, S.; Zhao, J.; Petek, H.; Rubio, A. Self-Energy and Excitonic Effects in the Electronic and Optical Properties of TiO_2 Crystalline Phases. *Phys. Rev. B* **2010**, *82* (4), 045207.

(20) Kronik, L.; Shapira, Y. Surface Photovoltage Phenomena : Theory , Experiment , and Applications. *Surf. Sci. Rep.* **1999**, *37*, 1–206.

(21) Ozawa, K.; Emori, M.; Yamamoto, S.; Yukawa, R.; Yamamoto, S.; Hobara, R.; Fujikawa, K.; Sakama, H.; Matsuda, I. Electron-Hole Recombination Time at TiO_2 Single-Crystal Surfaces: Influence of Surface Band Bending. *J. Phys. Chem. Lett.* **2014**, *5* (5), 1953–1957.

(22) Miaja-Avila, L.; Lei, C.; Aeschlimann, M.; Gland, J. L.; Murnane, M. M.; Kapteyn, H. C.; Saathoff, G. Laser-Assisted Photoelectric Effect from Surfaces. *Phys. Rev. Lett.* **2006**, *97*, 113604.

(23) Onda, K.; Li, B.; Zhao, J.; Jordan, K. D.; Yang, J. L.; Petek, H. Wet Electrons at the H_2O/TiO_2(110) Surface. *Science* **2005**, *308* (5725), 1154–1158.

(24) Zhukov, V. P.; Chulkov, E. V. Ab Initio Approach to the Excited Electron Dynamics in Rutile and Anatase TiO_2. *J. Phys. Condens. Matter* **2010**, *22* (43), 435802.

(25) Gundlach, L.; Ernstorfer, R.; Willig, F. Ultrafast Interfacial Electron Transfer from the Excited State of Anchored Molecules into a Semiconductor. *Prog. Surf. Sci.* **2007**, *82* (4–6), 355–377.

(26) Eagles, D. M. M. Polar Modes of Lattice Vibration and Polaron Coupling Constants in Rutile (TiO_2). *J. Phys. Chem. Solids* **1964**, *25* (11), 1243–1251.

(27) Traylor, J. G.; Smith, H. G.; Nicklow, R. M.; Wilkinson, M. K. Lattice Dynamics of Rutile. *Phys. Rev. B* **1971**, *3* (10), 3457–3472.

(28) Moser, S.; Fatale, S.; Krüger, P.; Berger, H.; Bugnon, P.; Magrez, A.; Niwa, H.; Miyawaki, J.; Harada, Y.; Grioni, M. Electron-Phonon Coupling in the Bulk of Anatase TiO_2 Measured by Resonant Inelastic X-Ray Spectroscopy. *Phys. Rev. Lett.* **2015**, *115*, 096404.

(29) Ellingson, R. J.; Asbury, J. B.; Ferrere, S.; Ghosh, H. N.; Sprague, J. R.; Lian, T.; Nozik, A. J. Dynamics of Electron Injection in Nanocrystalline Titanium Dioxide Films Sensitized with [Ru(4,4‘-Dicarboxy-2,2‘-Bipyridine)$_2$(NCS)$_2$] by Infrared Transient Absorption. *J. Phys. Chem. B* **1998**, *102* (98), 6455–6458.

(30) Kazempour, A. Quasiparticle Lifetimes in Rutile and Anatase TiO_2: GW Approximation. *Phys. Scr.* **2015**, *90* (2), 025804.

(31) Yeh, J. J.; Lindau, I. Atomi Subshel Photoionization Cross Sections and Asymmetry Parameters: $1 \leq Z \leq 103$. *At. Data Nucl. Data Tables* **1985**, *32* (l), 1.

(32) Xu, M.; Gao, Y.; Moreno, E. M.; Kunst, M.; Muhler, M.; Wang, Y.; Idriss, H.; Wöll, C. Photocatalytic Activity of Bulk TiO_2 Anatase and Rutile Single Crystals Using Infrared Absorption Spectroscopy. *Phys. Rev. Lett.* **2011**, *106* (13), 138302.

(33) Yamada, Y.; Kanemitsu, Y. Determination of Electron and Hole Lifetimes of Rutile and Anatase TiO_2 Single Crystals. *Appl. Phys. Lett.* **2012**, *101* (13), 133907.

(34) Zhang, L.; Zheng, Q.; Xie, Y.; Lan, Z.; Prezhdo, O. V.; Saidi, W. A.; Zhao, J.

Delocalized Impurity Phonon Induced Electron-Hole Recombination in Doped Semiconductors. *Nano Lett.* **2018**, *18* (3), 1592–1599.

(35) Shockley, W.; Read, W. T. Statistics of the Recombination of Holes and Electrons. *Phys. Rev.* **1952**, *87* (46), 835–842.